
DYNAMIC DATA ASSIMILATION OF MPAS-O AND THE GLOBAL DRIFTER DATASET

A PREPRINT

Derek DeSantis

CCS-2, W-13

Los Alamos National Laboratory

ddesantis@lanl.gov

Ayan Biswas

CCS-3

Los Alamos National Laboratory

ayan@lanl.gov

Earl Lawrence

CCS-6

Los Alamos National Laboratory

earl@lanl.gov

Phillip J. Wolfram

W-13

Los Alamos National Laboratory

pwolfram@lanl.gov

May 16, 2023

Keywords Data assimilation · Dynamic Mode Decomposition · Ocean Dynamics · E3SM · GDP

Abstract

In this study, we propose a new method for combining in situ buoy measurements with Earth system models (ESMs) to improve the accuracy of temperature predictions in the ocean. The technique utilizes the dynamics and modes identified in ESMs to improve the accuracy of buoy measurements while still preserving features such as seasonality. Using this technique, errors in localized temperature predictions made by the Model for Prediction Across Scales Ocean component (MPAS-O) can be corrected. We demonstrate that our approach improves accuracy compared to other interpolation and data assimilation methods. We apply our method to assimilate MPAS-O with the Global Drifter Program's in-situ ocean buoy dataset.

1 Introduction

In the field of Earth System Sciences, it is important to constantly improve the accuracy of measurements and models in order to better understand the Earth's climate. One way to analyze climate is through the use of powerful Earth system models (ESMs), such as the DOE's Energy Exascale Earth System Model (E3SM) [6]. ESMs provide estimates of state variables across a large number of grid cells, such as the Model for Prediction Across Scales Ocean component (MPAS-O), which is used in the E3SM and provides temperature estimates at different sized ocean cells [6, 9, 11]. Another method for studying climate is through direct in situ observations, such as those collected by satellites, towers, or ocean buoys. These observations are more accurate at specific locations, but are limited in coverage. An example of a highly resolved ocean buoy dataset is the Global Drifter dataset program (GDP) overseen by NOAA [5, 4]. In many cases, scientists use interpolation techniques to estimate state variables, such as temperature or salinity, between observations. Each of these approaches has its own advantages and disadvantages, and integrating both types of data can provide the greatest flexibility and predictive power [10].

Basis function models, which use linear combinations of continuous functions to estimate a state, are a flexible and computationally efficient method for solving non-stationary systems [2]. In these models, a set of basis functions are chosen or discovered, and the associated coefficient weights for an unknown function in the space are learned. In this work, we propose a new basis function model for data integration and compare its effectiveness to other data integration methods. We will explore three different methods for obtaining basis functions: 1) basis functions fit purely from in situ observations, 2) basis functions discovered through ESMs and fit to in situ data, and 3) our newly developed dynamic model, which builds on the second approach by weighting the basis functions according to extracted dynamical information from the ESM.

In the following sections, we provide background information and detail the techniques used in this study. In Section Three, we present the results of these methods for assimilating GDP data with MPAS-O and show that the dynamic method provides the best overall results in terms of mean squared error. We also discuss how the dynamic method is able to correct for biases within the MPAS model while simultaneously adjusting for temporal variations, which the other basis methods fail to capture.

2 Methods

2.1 Notation, Data set dimensions and variables

Throughout this study, let \mathcal{M} denote the physical domain of interest, while discrete times for buoy and model observations are denoted by t_j for $j = 1, 2, \dots, T$. In our study, \mathcal{M} will denote the Atlantic Ocean between latitudes $15^\circ - 55^\circ$ N and longitudes $260^\circ - 20^\circ$ E with a time increment of five days between each slice ($t_{j+1} - t_j$). The number of time slices will vary depending on the training problem, but examples we will consider are $T = 6, 18$, and 74 , corresponding to one month, one season, and one year, respectively. At each time t_j , there are N_j buoy measurements, and the total number of buoy measurements over the entire time period from t_1 to t_T is denoted by $N = \sum_{j=1}^T N_j$. We use $\{x_i\}_{i=1}^N \subset \mathcal{M}$ and $\{y_i\}_{i=1}^N \subset \mathbb{R}$ to represent the complete set of buoy locations and temperature measurements, respectively. For emphasis, the buoy measurements indexed by $\{(x_i, y_i)\}_{i=N_j}^{N_{j+1}-1}$ correspond to all the data at time t_j , and we use $(x_i(t_j), y_i(t_j))$ to refer to a single datum at time t_j . For a fixed set of sequential temporal observations, we let $[t_1 : t_T] = \{t_1, t_2, \dots, t_T\}$.

For the ESM data, there are L fixed grid cells $\{w_l\}_{l=1}^L$ that cover the domain \mathcal{M} . Each cell provides temperature measurements for each time t_1, \dots, t_T . Each buoy position $\{x_i\}_{i=1}^N \subset \mathcal{M}$ belongs to exactly one of the grid cells from the ESM. We let \hat{x}_i denote the index of the cell that buoy x_i belongs to. Similar to the notation used for the buoy data, we use $\{z_l(t_j)\}_{l=1}^L$ to represent the ESM temperature measurements at time t_j .

In this study, we will use the The Model for Prediction Across Scales Ocean component (MPAS-O) as our ESM and the Global Drifter Program (GDP) for ocean buoy data. MPAS-O is an ocean model that simulates ocean systems on time scales ranging from months to millenia and spatial scales as small as sub 1 kilometer [6]. Specifically, we will be using the V1 historical run of MPAS-O [3]. The GDP is a large array of more than 1000 satellite-tracked ocean buoys that measure ocean variables such as drift and sea surface temperature, and are commonly used in weather prediction [5, 4]. These two datasets have different temporal resolutions, so some time averaging within the GDP is required to match the MPAS-O. See the appendix for more details.

2.2 Basis Function Interpolation for Data Integration

Basis function interpolation is a useful method for data integration. In general, interpolation involves finding a function $F : \mathcal{M} \rightarrow \mathbb{R}$ such that $F(x_i) \cong y_i$ for $i = 1, \dots, N$, where \mathcal{M} is the domain of interest, $\{x_i\}$ are known points in \mathcal{M} , and $\{y_i\}$ are corresponding values. One approach to constructing F is to represent it as a linear combination of simple basis functions $\phi_j : \mathcal{M} \rightarrow \mathbb{R}$:

$$F(x) = \sum_{j=1}^M a_j \phi_j(x).$$

To perform a basis function interpolation, we first select or discover the basis functions $\{\phi_j\}_{j=1}^M$, and then solve the regression problem:

$$y_i \cong F(x_i) = \sum_{j=1}^M a_j \phi_j(x_i).$$

This can be written in matrix form as

$$\vec{y} \cong \Phi \vec{a}, \quad (1)$$

where $\Phi_{i,j} = \phi_j(x_i)$, $\vec{y} = (y_1, \dots, y_N)^T$, and $\vec{a} = (a_1, \dots, a_M)^T$. The least-square solution to Equation 1 is obtained by taking the Moore-Penrose inverse of Φ on both sides:

$$\vec{a} \cong \Phi^\dagger \vec{y}.$$

The Moore-Penrose inverse can be computed using the singular value decomposition (SVD) of Φ . If the SVD of Φ is given by $\Phi = U\Sigma V^T$, then the Moore-Penrose inverse is $\Phi^\dagger = V\Sigma^\dagger U^T$, where Σ^\dagger is found by taking the transpose and inverting each entry on the diagonal of Σ . In many cases, the matrix Φ may be ill-conditioned, in which case regularization is needed. Optimization is performed over a range of regularization parameters to find the best fit on the training data. Once the coefficients \vec{a} have been obtained, the model can be tested for accuracy on the test data.

Data integration is achieved through basis function interpolation by selecting basis functions or deriving them from the ESM. Interpolation is then performed using the buoy observations $\{(x_i, y_i)\}$. In this work, we will consider different types of basis functions and different temporal ranges for the interpolation. The basis functions do not need to be orthogonal. In the next section, we will describe our choice of models in more detail.

2.3 Radial Basis Functions - Purely Buoy Data Driven

One approach to deriving F is to use only the observations $\{(x_i, y_i)\}$ and ignore the ESM data completely. In this case, a natural choice is to use radial basis functions (RBFs) for ϕ_j . Specifically, we can define $\phi_j(x) = \psi(|x - \mu_j|)$, where $\psi: M \rightarrow \mathbb{R}$ is a fixed function (such as a Gaussian) and $\mu_j \in \mathcal{M}$ are the mean or center points. Often, the RBF chosen has a tuning parameter ϵ , such as the standard deviation in a Gaussian. In addition to the RBFs, it is also common to include a polynomial term $P(x)$ of degree D to capture mean behavior. Therefore, $F: M \rightarrow \mathbb{R}$ can be expressed as:

$$F(x) = P(x) + \sum_{j=1}^M a_j \phi_j(x) \quad (2)$$

In this approach, the user must choose the number of basis functions M , the centers μ_j , the basis functions ϕ_j , and the degree of the interpolating polynomial D . A common choice for M and μ_j is to use the size of the training set N and the locations of the training set, and is the practice adopted here. For more information on RBFs, see [1, 12].

2.4 Static ESM Mode Decompositions for Basis

In this subsection, we describe how to obtain basis functions $\{\phi_j\}_{j=1}^M$ from the ESM data. We consider two methods for extracting spatially coherent functions, or modes of variability, that are faithful to the spatial grid $\{w_l\}_{l=1}^L$ provided by the ESM. First, we describe how to obtain these modes, and then discuss how to use them to produce basis functions.

For each time $t \in [t_1 : t_T]$, the ESM data $z_l(t)_{l=1}^L$ provides an estimate of the temperature distribution over the spatial domain \mathcal{M} at time t . This data can be arranged into an $L \times T$ matrix Z .

The Singular Value Decomposition (SVD) can be used to directly obtain modes [7]. Let $Z \cong U\Sigma V^T$ be the rank- M SVD of Z . The M left singular vectors in the columns of $U = [U_1, U_2, \dots, U_M] \in \mathbb{R}^{L,M}$ form a set of (orthogonal) spatial modes for Z .

Another method for extracting modes is the Dynamic Mode Decomposition (DMD) [8, 13]. Unlike SVD, the derived modes are not orthogonal, which allows DMD to capture more physically relevant modes within the decomposition (at the potential cost of parsimony). The process of computing DMD modes $\{U_j\}_{j=1}^M$ is more involved than SVD and is briefly summarized in the appendix.

Since each point $x \in \mathcal{M}$ belongs to one of the grid cells $\{w_l\}_{l=1}^L$ of the ESM, any mode decomposition of Z can be used for interpolation by evaluation. Specifically, let \hat{x} denote the cell index $l = 1, \dots, L$ that the point x belongs to, and $\{U_j\}_{j=1}^M \subset \mathbb{R}^L$ be modes of Z . We define the **static (SVD or DMD) mode basis** as

$$\phi_j(x) := U_{\hat{x},j}$$

for each $j = 1, \dots, M$. In other words, the static mode basis is simply the spatial modes obtained through the modal decomposition (SVD or DMD).

2.5 Dynamic ESM Mode Decompositions for Basis

Both of the mode-based decompositions discussed in the previous subsection also include additional dynamical information that has not been utilized. In this subsection, we present a method for incorporating this information into basis function interpolation.

In SVD, the left singular vectors $U = [U_1, \dots, U_M] \in \mathbb{R}^{L,M}$ represent spatial patterns, while the right singular vectors $V = [V_1, \dots, V_T] \in \mathbb{R}^{T,M}$ represent the intensity of each of the M patterns across the T time slices. Similarly, DMD produces its M DMD modes $U = [U_1, \dots, U_M] \in \mathbb{R}^{L,M}$ and their associated dynamics (intensity across time), as described in the appendix. For either mode decomposition, let $\alpha_j(t)$ describe the dynamics of the DMD mode U_j .

Each buoy measurement (x_i, y_i) is taken at a specific time $t \in [t_1 : t_T]$. More generally, we can associate each point $x \in \mathcal{M}$ with a time $t \in [t_1 : t_T]$ at which we want to provide interpolation. We define the **dynamic (SVD or DMD) mode basis** as

$$\phi_j(x) := \alpha_j(t)U_{\hat{x},j}$$

for each $j = 1, \dots, M$ ¹. In other words, the dynamic mode basis is obtained from the static mode basis by weighting the static mode at an observation by its intensity at the time of the observation.

2.6 MPAS-O - Purely ESM Data Driven

As a baseline, we will compare the performance of our basis models to the ESM, which provides an approximation of the surface temperature over \mathcal{M} . While ideally the ESM would accurately represent the in-situ buoy measurements, we hope that basis function interpolation to improve the model in expectation. The ESM baseline is computed by finding the ESM cell that each buoy belongs to and comparing the model's output to the buoy measurement:

$$z_{\hat{w}_i}(t_j) - y_i(t_j).$$

3 Results

Figure 1 displays the test errors for the different models for three different now-cast time lengths T . Each model from Section 2 is fit for lengths $T = 6, 18$ or 74 to represent one month, three months, or one year. The model is fit on 80% of the data and tested on the remaining 20% to produce an error measurement. A distribution of errors for each model, and each time T is created by choosing different starting times t_1 . A total of 100 start times t_1 are chosen uniformly spaced one month apart from one another. The left side of Figure 1 displays the box and whisker plot for each of the error distributions of each model at each time length T . The right side of Figure 1 displays the top three best performing models.

One key takeaway from Figure 1 is that in each scenario, the dynamic basis interpolation using DMD modes outperforms MPAS across all time scales. While the RBF model performs better than the fully dynamic DMD model on the short timescale of one month, it performs worse on longer timescales. Another important observation is that the SVD methods perform better on longer timescales. On the short timescale of one month, both SVD methods have a poor fit, but on the one-year fit, the dynamic SVD begins to outperform the RBF model. Given the dominance of the fully dynamic DMD model over the other basis models, we will focus on its benefits in future analysis.

Next, we will perform a deeper analysis of the model performance over a single year. For demonstration purposes, we have selected the date range of Jan. 1st, 2008 to Jan 1st, 2009 to display here². Figure 2(a) shows how the test error is improved by adding the dynamic component to the DMD mode decomposition. The DMD basis decomposition has a somewhat bimodal error, indicating that the model has over- or undercompensated for SST in some regions. Figure 2(b) illustrates that this is due to seasonality - the basic DMD model has discovered a mean state to represent the temperature, missing the extremes of both summer and winter. Weighting the modes by their dynamics removes these biases, producing a normally distributed error with a much lower standard deviation. Figure 2(c) shows that MPAS has a hot temperature bias, pushing the distribution's mean into the negatives. This is further seen in Figure 2(d), where MPAS appears to have a negative temperature bias across the whole year.

Finally, we will analyze the spatial distribution of the discovered temperature field to ensure that it adheres to known physics. Figure 3(a) shows the average yearly temperature field interpolation provided by the fully dynamic DMD model, while figure (b) displays the difference between the fully dynamic DMD and MPAS. Figure 3(c) shows the temperature distribution for both the fully dynamic DMD basis model and MPAS. Figure 4(a) plots the location and temperature of the test buoys across the year. Figure 4(b) and (c) show the test errors of the fully dynamic DMD and MPAS models, respectively. The buoy errors in Figure 4 show that MPAS has a clear latitudinal temperature bias,

¹Note that since the dynamic information $\alpha_j(t)$ has already been captured, the added complexity compared to the static method is $\mathcal{O}(1)$ per observation.

²While we focus on Jan. 1st, 2008 to Jan 1st, 2009, the results presented here are representative of the general year-long phenomenon. The following discussion and analysis can be applied to any time slice, since the fully dynamic models have temporal information.

whereas the fully dynamic DMD has relatively uniform errors. Figures 3 and 4 show that the interpolation method discovered by the fully dynamic DMD is not dissimilar from the physical model MPAS-O. The primary difference is a lower temperature in the fully dynamic DMD model in the higher latitudes (the location where MPAS-O has a large temperature bias). This suggests that the dynamic model is learning something that is physically consistent with MPAS, while simultaneously improving upon its ground truth accuracy as measured by the GDD.

4 Discussion

RBF methods can provide an arbitrary, unrealistic goodness of fit by adding more nodes. Since the RBF centers are chosen from the buoy locations, this model is sensitive to time scales. As noted above, on longer time lengths RBF begins to perform more poorly compared to other models. This is likely due to the fact that RBF works to find the best fits at the time the buoy measurements are made. As a result, if longer timescales are included, the RBF model will fit a dataset with nearby buoy measurements with seasonal variability, such as Winter and Summer measurements in close proximity. This lack of physical knowledge makes the fit rather unrealistic, as nearby nodes in the model compete for what the "real" value should be, resulting in high spatial variability.

The SVD works to reduce noise, and in noise-dominated cases can be effectively swamped in such a way that it does not provide clear basis modes. As discussed in the previous section, the SVD models perform extremely poorly on short timescales of one to three months. On such timescales, the high-frequency data can dominate the signal, causing poor predictions. This might be due in part to the fact that SVD assumes orthogonal, non-interacting modes, which are poor at capturing variability of shorter timescales.

DMD provides better estimates of spatio-temporal evolution than SVD. This could be due in part to the fact that DMD modes have dynamics described by the growth and decay of eigenvalues. As such, the spatial modes are unambiguously associated with particular months, seasons, cycles, etc. Consequently, DMD can intrinsically adapt to seasonal changes better. While SVD does provide dynamic information, DMD is explicitly built to extract different modes of variability. Climate change identification and predictions can be made with DMD, whereas the SVD's lack of flexibility and susceptibility to noise make it less accurate because it is not temporally adaptable. That said, the static mode decomposition using DMD modes appears to get worse as you increase the time window. This is due to the fact that the weight of the mean state still dominates, as shown in Figure 2 and discussed above.

The key discovery from the previous section is that adding available dynamics, specifically to the DMD method of interpolation, improves predictive skill while correcting for mean biasing (Figure 1). We want to use the dynamic models when the time includes seasonal features (longer time scales). This is because the fully dynamic DMD captures different time scales and reweights them into the model, whereas other basis models either do an arbitrary fit (RBF) or capture means (Figure 2). The fully dynamic DMD method also improves the biases of MPAS as seen by combining the buoy and spatial pictures of Figures 3 and 4. As noted above, the fully dynamic DMD model corrects for the temperature bias within MPAS-O at higher latitudes. The discovered DMD modes capture the dynamics of MPAS-O, while having the flexibility to be reweighted to match the real observational data.

5 Conclusion

In this paper, we compared various methods for interpolating ocean buoy data. In particular, we are interested in the data assimilation of the ESM ocean data MPAS-O with in situ GDP buoy data. Our analysis showed that the performance of an interpolation method depends on the time scale being considered. Some methods may be more effective for short time scales, while others may perform better on longer time scales. We found that adding dynamic information, specifically to the DMD method, improves predictive accuracy and corrects for biases on longer time scales with seasonal dynamics. The DMD with dynamics was consistently the best performer among all methods, improving the ESM MPAS-O. We demonstrated that the DMD with dynamics is not overfitting and is making reasonable spatial predictions while also correcting for biases in MPAS. Therefore, we conclude that the DMD with dynamics is the superior method among those examined.

This type of dynamic decomposition for interpolating ocean data that can adapt to both high and low frequency information show great potential. The dynamic data assimilation technique discussed here allow for more data-rich analysis that could be useful for understanding evolving dynamics. Further applications of these approaches may be useful and application to in-situ analysis or data assimilation appear most promising.

6 Acknowledgements

Research presented in this article was supported by the Laboratory Directed Research and Development program of Los Alamos National Laboratory under project number 20200065DR. DD was supported by the DOE Office of Science Biological and Environmental Research (BER), as a contribution to the HiLAT-RASM project. MPAS-O V1 were obtained from the Energy Exascale Earth System Model project, sponsored by the U.S. Department of Energy, Office of Science, Office of Biological and Environmental Research. Satellite-tracked drifting buoy data are available from the Global Drifter Program (GDP), with support from their website (<ftp://ftp.aoml.noaa.gov/pub/phod/buoydata/>).

7 Appendix

7.1 Time Filtering GDD Data to MPAS-O

The MPAS-O and GDP datasets are on different temporal resolutions (Five day averages versus six hour). We therefore coarse-grained the GDP data in time to fit the temporal resolution of MPAS. Given two sequential MPAS-O time snapshots t and $t + 1$, all the GDP buoy data is collected within each of those five days. For each buoy, the average spatial location and temperature is then recorded and used as $\{x_i(t)\}$ and $\{y_i(t)\}$.

7.2 DMD Short Summary

In the Dynamic Mode Decomposition (DMD), the system is assumed to be evolved in an approximately linear fashion:

$$\tilde{z}_{t+1} \cong A\tilde{z}_t. \quad (3)$$

This is effectively the solution of a forward-in-time spatially discrete solver, where A can contain physical operators such as advection, diffusion, etc. The value in this form is that growth, decay, and oscillatory behavior is all immediately represented, albeit pseudo-linearly from one time step to the next. Given this interpretation, one can think of A as effectively a learned, empirical physically-meaningful discretization.

Let Z_1 and Z_2 be the matrices given by $Z_1 = [\tilde{z}_1 \tilde{z}_2 \dots \tilde{z}_{T-1}]$ and $Z_2 = [\tilde{z}_2 \tilde{z}_3 \dots \tilde{z}_T]$. The goal is to find a good approximation \tilde{A} of the matrix A that represents this system. This can be cast as the following matrix problem:

$$Z_2 \cong AZ_1 \quad (4)$$

The least square solution to Equation 4 is found by taking the Moore-Penrose inverse:

$$A \cong Z_2 Z_1^\dagger.$$

Since A is a square matrix, one can consider the eigen-decomposition of A :

$$AU = U\Lambda \quad (5)$$

The eigenvectors and eigenvalues (u_j, λ_j) of the A are the **DMD modes and eigenvalues** respectively.

For systems with a large number of data points L , this direct method isn't tractable since A is a $L \times L$ square matrix. Therefore different methods are designed to 1) solve Equation 4 while 2) providing a reduced order model at the same time. Among the most simple and popular methods for doing this is the SVD-based method:

1. Compute the rank M SVD of $Z_1 = W\Sigma V^T$.
2. Consider $\tilde{A} := W^T AW$. Then \tilde{A} is $M \times M$, and since it is unitarily equivalent to A , has the same eigenvalues with eigenvectors ξ of \tilde{A} related to A via $W\xi$.
3. Note that since $Z_2 \cong AZ_1 = AW\Sigma V^T$, after multiplying by W^T and rearranging we have

$$\tilde{A} = W^T AW = W^T Z_2 V \Sigma^{-1}.$$

In other words, \tilde{A} can be computed directly from the data and SVD of Z_1 .

4. Compute eigenvectors and eigenvalues $\{\tilde{u}_j, \lambda_j\}$ of the much smaller $M \times M$ matrix \tilde{A} .
5. The j' th DMD mode is computed as $u_j := W\tilde{u}_j$.

Other methods for approximating the DMD modes based off SVD exist, such as exact DMD. See [13].

The DMD modes and eigenvalues can be used to derive dynamical information analogous with the right singular vectors of SVD. By iteratively applying Equation 3, we find that

$$\tilde{z}_{t+1} \cong A^t \tilde{z}_1 \quad (6)$$

Write \tilde{z}_1 in the basis provided by the modes Ψ :

$$\tilde{z}_1 = \Psi \vec{b}. \quad (7)$$

Then combining Equations 5, 6 and 7 we see that

$$\tilde{z}_{t+1} \cong A^t \tilde{z}_1 = A^t \Psi \vec{b} = \Psi \Lambda^t \vec{b}.$$

Hence, we have represented the state of the system in terms of a DMD mode expansion with temporal evolution on the DMD eigenvalues. The time series $\{(\lambda_j^t b_j)_{t=1}^T\}_{j=1}^M$ are referred to as the **DMD dynamics** for the j 'th mode ψ_j .

References

- [1] Martin D Buhmann. Radial basis functions. *Acta numerica*, 9:1–38, 2000.
- [2] Noel Cressie, Matthew Sainsbury-Dale, and Andrew Zammit-Mangion. Basis-function models in spatial statistics. *arXiv preprint arXiv:2202.03660*, 2022.
- [3] DOE E3SM Project. Energy exascale earth system model v1.0. [Computer Software] <https://doi.org/10.11578/E3SM/dc.20180418.36>, apr 2018.
- [4] S Elipot, A Sykulski, R Lumpkin, L Centurioni, and M Pazos. Hourly location, current velocity, and temperature collected from global drifter program drifters world-wide. *Accession*, 248584:v1, 2022.
- [5] Shane Elipot, Adam Sykulski, Rick Lumpkin, Luca Centurioni, and Mayra Pazos. A dataset of hourly sea surface temperature from drifting buoys. *arXiv preprint arXiv:2201.08289*, 2022.
- [6] Jean-Christophe Golaz, Peter M Caldwell, Luke P Van Roekel, Mark R Petersen, Qi Tang, Jonathan D Wolfe, Gita Abeshu, Valentine Anantharaj, Xylar S Asay-Davis, David C Bader, et al. The doe e3sm coupled model version 1: Overview and evaluation at standard resolution. *Journal of Advances in Modeling Earth Systems*, 11(7):2089–2129, 2019.
- [7] Nicholas J Higham. *Accuracy and stability of numerical algorithms*. SIAM, 2002.
- [8] J Nathan Kutz, Steven L Brunton, Bingni W Brunton, and Joshua L Proctor. *Dynamic mode decomposition: data-driven modeling of complex systems*. SIAM, 2016.
- [9] Mark R Petersen, Xylar S Asay-Davis, Anne S Berres, Qingshan Chen, Nils Feige, Matthew J Hoffman, Douglas W Jacobsen, Philip W Jones, Mathew E Maltrud, Stephen F Price, et al. An evaluation of the ocean and sea ice climate of e3sm using mpas and interannual core-ii forcing. *Journal of Advances in Modeling Earth Systems*, 11(5):1438–1458, 2019.
- [10] Rolf H Reichle. Data assimilation methods in the earth sciences. *Advances in water resources*, 31(11):1411–1418, 2008.
- [11] Todd Ringler, Mark Petersen, Robert L Higdon, Doug Jacobsen, Philip W Jones, and Mathew Maltrud. A multi-resolution approach to global ocean modeling. *Ocean Modelling*, 69:211–232, 2013.
- [12] Claude Sammut and Geoffrey I Webb. *Encyclopedia of machine learning*. Springer Science & Business Media, 2011.
- [13] Jonathan H Tu. *Dynamic mode decomposition: Theory and applications*. PhD thesis, Princeton University, 2013.

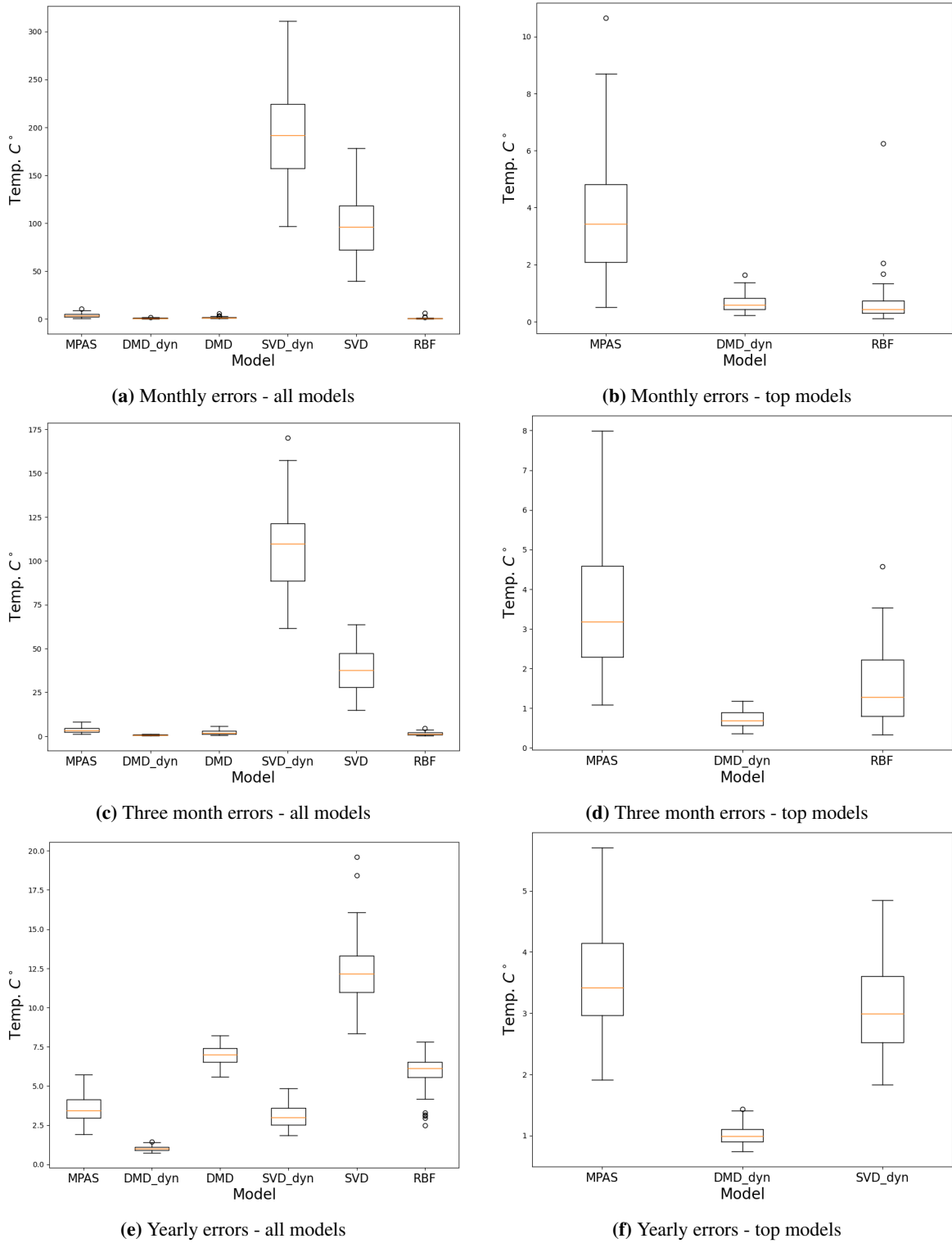


Figure 1: Figures (a), (c), (e) display the distribution of errors for all the models fit over one month, three month, and one year time windows. Figures (b), (d), (f) show the top three models from distributions.

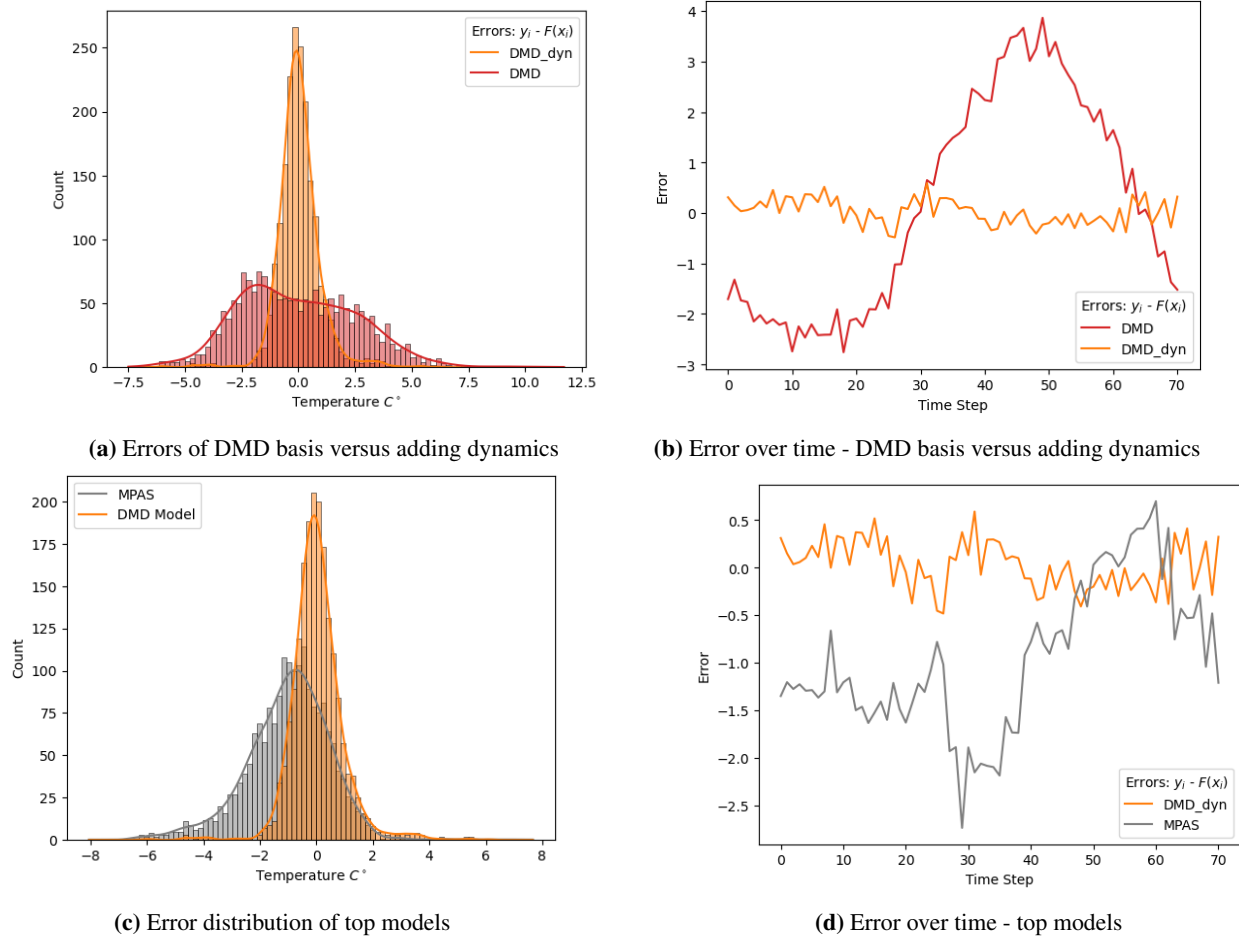
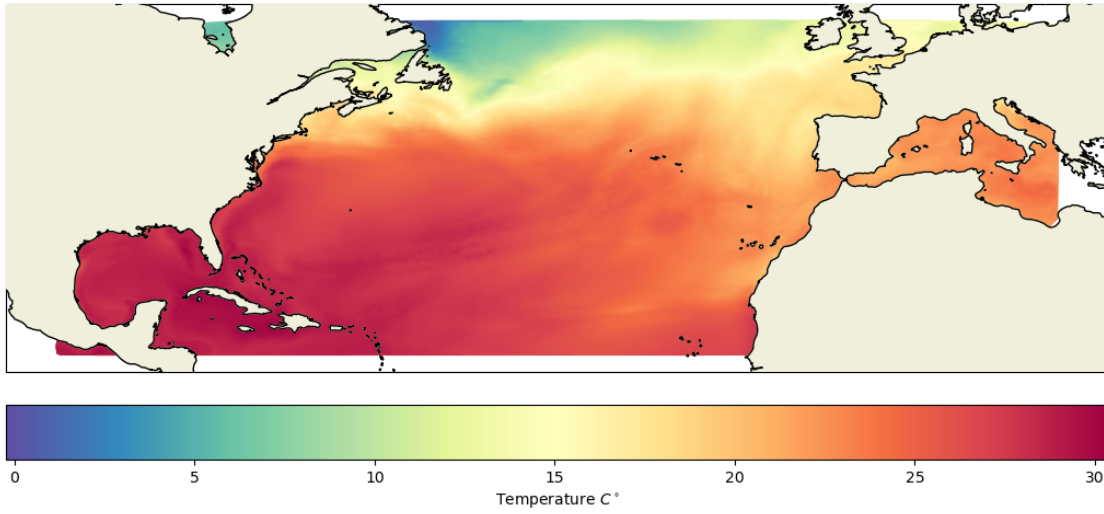
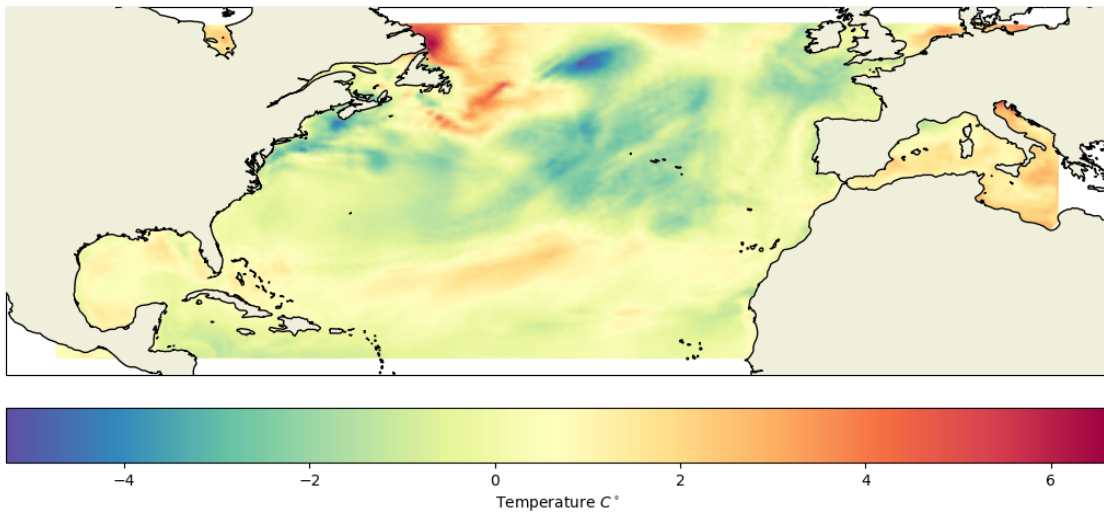


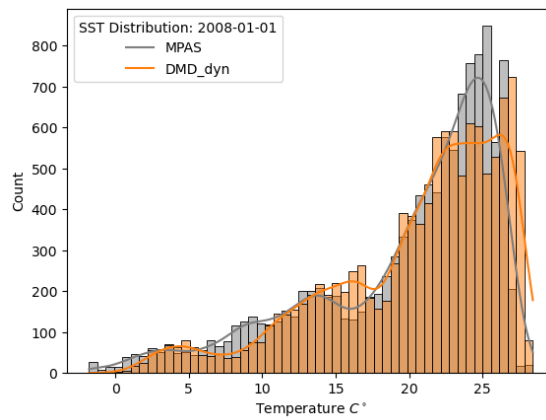
Figure 2: Errors of models for time period Jan. 1st 2008-Jan 1st 2009. Plots (a) and (c) display error distributions for different models. Plots (b) and (d) compute the average error on each of the five day time slices to explore inability to capture seasonality/baises.



(a) Fully dynamic DMD basis interpolation



(b) Difference between fully dynamic DMD basis and MPAS: $F_{\text{MPAS}}(x_i) - F_{\text{DMD_dyn}}(x_i)$



(c) SST distribution of MPAS versus fully dynamic DMD basis

Figure 3: Average yearly temperature comparison of fully dynamic DMD versus MPAS-O for time period Jan. 1st 2008-Jan 1st 2009

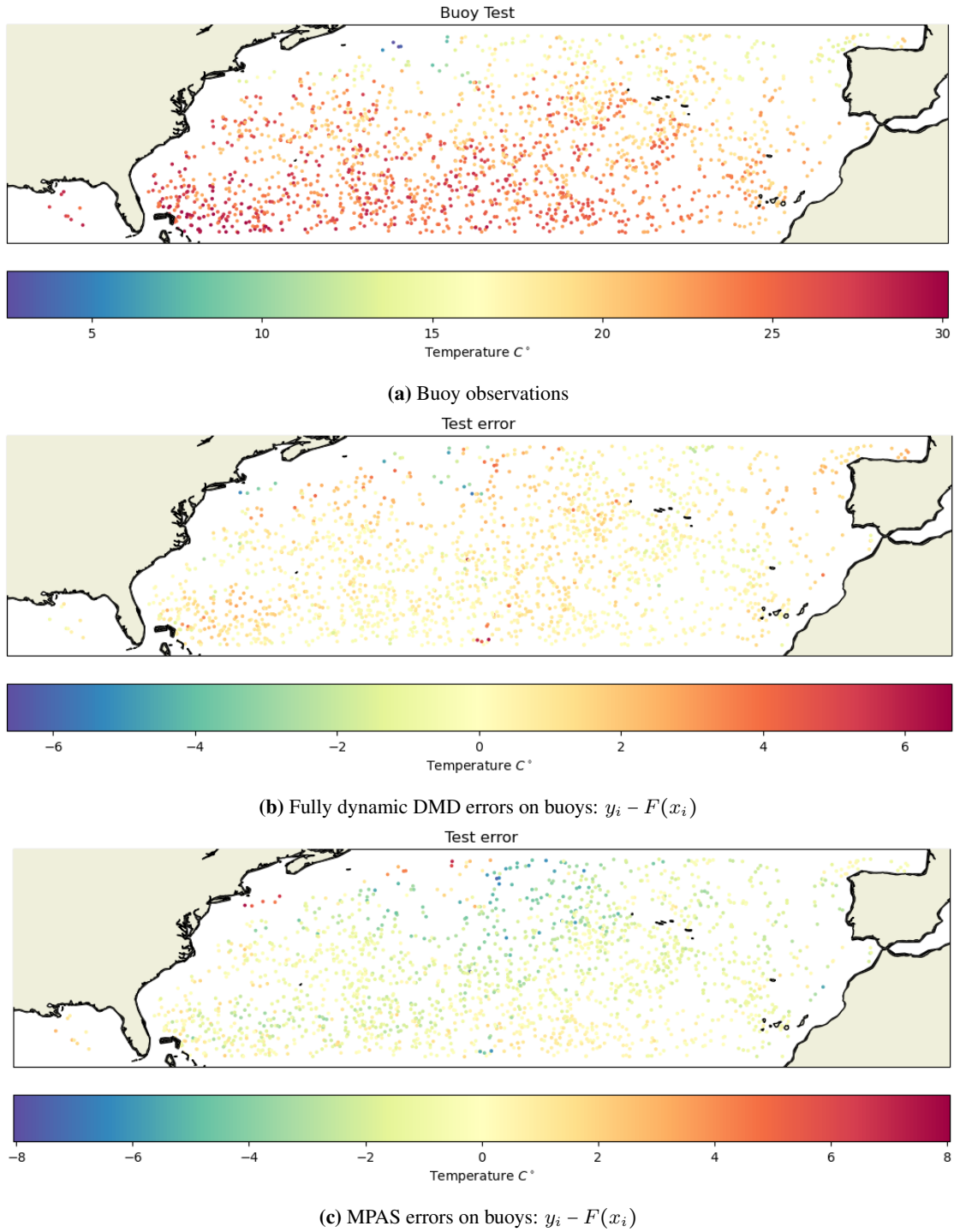


Figure 4: (a) Buoy observations, with (b) Fully dynamic DMD errors and (c) MPAS errors on test buoys for year Jan. 1st 2008-Jan 1st 2009.